Calculation of equilibrium lattice parameters and the heat of mixing for the system Au/Pd by the relativistic Korringa-Kohn-Rostoker coherent-potential-approximation method

P. Weinberger, J. Kudrnovsky, and J. Redinger
Institut für Technische Elektrochemie, Technical University of Vienna, Getreidemarkt 9/158, A-1060 Vienna, Austria

B. I. Bennett and A. M. Boring
Los Alamos National Laboratory, Los Alamos, New Mexico 87545
(Received 4 November 1992; revised manuscript received 19 March 1993)

Using the all-electron fully relativistic Korringa-Kohn-Rostoker coherent-potential-approximation method self-consistent total-energy calculations were performed for the system Au/Pd. The calculated equilibrium lattice constants are in fairly good agreement with the experimental data. In particular, microscopic reasons for the breaks in the variation of the lattice constants with concentration can be derived from the results. Since the calculations were carried out self-consistently for a maximum angular momentum quantum number of 2 as well as 3, an interesting quantitative comparison for the alloy total energies, spectral densities, and properties related to the Fermi energy or Fermi surface can be presented.

I. INTRODUCTION

The calculation of ground state total energies for ordered systems within the local density functional approximation (LDA) as a function of the lattice spacing has become a fairly standard procedure over the past few years. To a lesser extent such calculations have been performed on a fully relativistic scale. For obvious computational reasons it became customary in many applications to treat only the core states relativistically and to use a more or less sophisticated pseudorelativistic or completely nonrelativistic approach for the valence bands. For substitutionally disordered alloys even nonrelativistic total-energy calculations are still rather rare, and up to now they are confined to a few systems.[1] The reason for this late start in the computation of the energetics in alloy theory is rather simple: Not only do the equilibrium lattice constants have to be computed within less than about 1%, as compared to experiment, but also their variation with concentration has to be described adequately. Since this variation usually changes over the whole range of concentrations by about 5% of the lattice constants of the alloy partners, this becomes a difficult numerical problem. Carrying out such calculations on a fully relativistic scale is even more cumbersome. However, in many cases, including famous systems such as Cu/Au, Cu/Pt, or Ni/Pt, to name only a few, a fully relativistic approach is definitely required for an adequate treatment of alloys.

Au/Pd is particularly demanding, since by alloying Au with an increasing concentration of Pd, the Fermi energy moves out of the *sp* band into the edge of the *d* band, causing a very sudden and rapid increase in the linear coefficient of the specific heat[4] (around 60% Au) and a change in the slope of the experimental lattice constants.[5] In addition, it is well known that the edge of the *d* band in pure Pd is characterized by sharp peaks in the density of states (DOS) near the Fermi energy, which also show up in the alloy for low Au concentrations. As will be shown, the movement of the Fermi energy through the top sharp peak around 30% Au is the cause for the second break in the observed lattice parameters. For previous non-self-consistent calculations for the system Au/Pd see Refs. 2 and 3.

II. COMPUTATIONAL DETAILS

In the present study, two complete sets of fully relativistic Korringa-Kohn-Rostoker coherent-potential-approximation (KKR-CPA) calculations[6,7] have been carried out over a wide range of concentrations: one using consistently a maximum angular momentum quantum number of $l_{\max} = 2$, and one using $l_{\max} = 3$. This yields an interesting quantitative comparison not only for the total energies, but also for quantities related to the Fermi surface, not given previously in the literature. For each concentration ($c_{\mathrm{Au}} = 0.20, 0.30, 0.40, 0.50, 0.60, 0.70, 0.75, 0.80$) the lattice constant was varied from 7.35 a.u. to 7.70 a.u. in steps of 0.05 a.u.

A. CPA self-consistency

All **k**-space integrations were performed using the 21 special directions of Fehlner and Vosko.[8] The CPA equations were solved[9] along the real axis of the energy with an accuracy of 10^{-5}. It should be noted that for an fcc lattice and $l_{\max} = 2$ the CPA condition consists of seven equations associated with the following channels: (1) $\Gamma_6^+(s^{1/2})$, (2) $\Gamma_6^-(p^{1/2})$, (3) $\Gamma_8^-(p^{3/2})$, (4) $\Gamma_7^+(d^{5/2})$, (5) $\Gamma_8^+(d^{3/2})$, (6) $\Gamma_8^+(d^{5/2})$, and (7) $\Gamma_8^+(d^{3/2}/d^{5/2})$. For $l_{\max} = 3$ ten additional channels have to be considered: (8) $\Gamma_7^-(f^{5/2})$, (9) $\Gamma_8^-(f^{5/2})$, (10) $\Gamma_6^-(f^{7/2})$, (11) $\Gamma_7^-(f^{7/2})$, (12) $\Gamma_8^-(f^{7/2})$, (13) $\Gamma_7^-(f^{5/2}/f^{7/2})$, (14)

 ©1993 The American Physical Society

$\Gamma_8^-(f^{5/2}/f^{7/2})$, (15) $\Gamma_6^-(p^{1/2}/f^{7/2})$, (16) $\Gamma_8^-(p^{3/2}/f^{5/2})$, (17) $\Gamma_8^-(p^{3/2}/f^{7/2})$. Channels 7, 13, and 14 are "spin-flip" channels, while channels (15) to (17) couple p-like states to f-like states. Quite clearly an $l_{\max} = 2$ calculation is easiest to perform since the size of the KKR matrix is only 18×18, while for $l_{\max} = 3$ the matrix is already 32×32, requiring considerably more computing time.

B. LDA self-consistency

In each LDA iteration the component core charge densities were recalculated fully relativistically, imposing the convergence criterion for core one-electron energies of less than 10^{-9} Ry. The obtained results correspond therefore to a truly "all-electron" approach. The LDA functional approximation used was that of Gunnarsson and Lundqvist.[23] For all lattice constants a the muffin-tin radius $R_{\rm mt}$ is the inscribed Wigner-Seitz radius, $R_{\rm mt} = a/\sqrt{8}$. The radial integrations required to evaluate total charges, etc., were performed for exactly the same number of radial mesh points. For the energy integrations (along the real axis) both trapezoidal and cubic spline forms were used. The difference between these two numerical approaches usually was considerably less than 0.5 mRy. The Fermi energy was obtained by integrating the DOS rather than using Lloyd's formulation of the integrated DOS,[10,7] since the same l-convergence as for the charge densities is guaranteed.

In both cases, namely for the $l_{\max} = 2$ and the $l_{\max} = 3$ calculations, the component charge densities were iterated until each of the component total energies $\langle E_\alpha \rangle$, α =Au,Pd, and the averaged total energy $\langle E \rangle$[11]

$$\langle E \rangle = \sum_{\alpha=A,B} c_\alpha \langle E_\alpha \rangle \quad (1)$$

varied less than about 0.5 mRy in two to three consecutive iterations. Considering that finite radial and energy grid sizes are used, this gives an overall accuracy of about 1 mRy for $\langle E \rangle$ when varying the lattice constant. Since the total energy of Au differs from that of Pd by nearly 28 000 Ry, this implies that the calculations had to be accurate to about half the ninth significant figure. In order to achieve this precision, the Fermi energy between consecutive LDA iterations had to settle down to a difference of less than 0.1 mRy.

III. RESULTS AND DISCUSSION

A. Spectral densities

As can been seen from Fig. 1 of Ref. 12 for $c_{\rm Au} > 0.6$ the Fermi energy lies well above the d band, the Au $d^{3/2}$−partial local density of states (PDOS) shows the characteristic pattern of peaks known from pure Au, while the Pd peaks show "spin-orbit" split virtual bound states. For $Au_{60}Pd_{40}$ the Fermi energy is located at the very edge of the d band. For $c_{\rm Au} < 0.6$ the Pd d-like PDOS's show a characteristic peak rising in amplitude just below the Fermi energy. For $Au_{30}Pd_{70}$ the Fermi energy almost coincides with this very sharp peak. For $c_{\rm Au} = 0.20$ the Fermi energy moves into the valley between the last two peaks in the Pd d-like PDOS. It can also be seen from this figure that for $Au_{25}Pd_{75}$ the Au $d^{3/2}$−PDOS already resembles the characteristic features of a virtual bound state (i.e., it is characterized by a breakdown of dispersion), while the Au $d^{5/2}$−PDOS is still fairly broad. For very low Au concentrations, $c_{\rm Au} \ll 0.25$, two "spin-orbit" split virtual bound states will characterize the Au PDOS.

B. Total energies

For Au concentrations below 0.6, locating the position of the Fermi energy is quite delicate. This implies that since the nonresonant f channels are missing (these contribute in an $l_{\max} = 3$ calculation to the total charges), any $l_{\max} = 2$ calculation will put the Fermi energy at too high an energy. Figure 1 shows the $l_{\max} = 2$ and $l_{\max} = 3$ potential curves for $Au_{50}Pd_{50}$ and $Au_{70}Pd_{30}$. In absolute values the $l_{\max} = 3$ potential curves are lower in energy by more than 30 mRy relative to the $l_{\max} = 2$ curves. As can be seen from Fig. 1, the $l_{\max} = 2$ equilibrium lattice parameters are definitely wrong and therefore also their variation with respect to the concentration. It should be noted that in Fig. 1 all entries correspond to calculated values and not to a fit.

In Fig. 2 the calculated ($l_{\max} = 3$) equilibrium lattice constants are compared to the experimental ones,

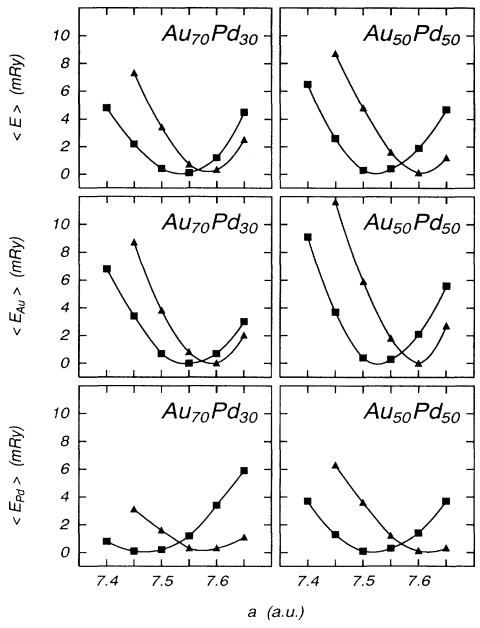

FIG. 1. (a) $l_{\max} = 2$ (triangles) and $l_{\max} = 3$ (squares) averaged total-energy potential curves for $Au_{70}Pd_{30}$ (left) and $Au_{50}Pd_{50}$ (right). (b) $l_{\max} = 2$ (triangles) and $l_{\max} = 3$ (squares) component total-energy potential curves for Au in $Au_{70}Pd_{30}$ (left) and $Au_{50}Pd_{50}$ (right). (c) $l_{\max} = 2$ (triangles) and $l_{\max} = 3$ (squares) component total-energy potential curves for Pd in $Au_{70}Pd_{30}$ (left) and $Au_{50}Pd_{50}$ (right).

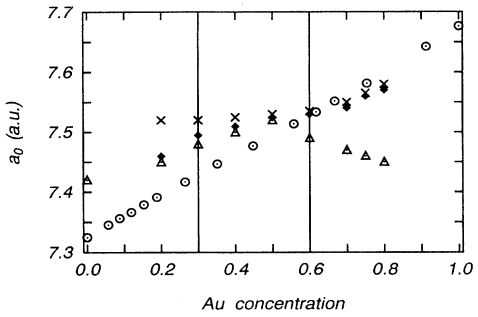

FIG. 2. Calculated ($l_{\max} = 3$) values of a_0 (squares), a_0^{Au} (triangles), and a_0^{Pd} (circles) as compared to the experimental equilibrium lattice constants (Ref. 5) (asterisks), reduced to zero temperature. The two breaks in the linear behavior of the experimental lattice constants with respect to the concentration, namely at 30% and 60% Au, are indicated by vertical dashed lines. For comparison for pure Pd the theoretical value of Moruzzi, Janak, and Williams (Ref. 15) is shown.

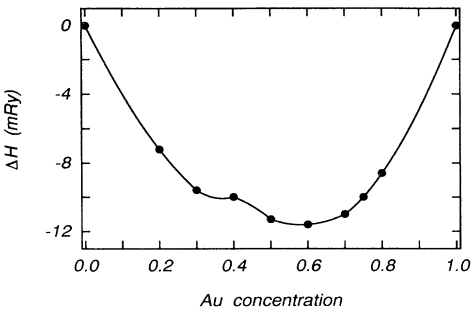

FIG. 3. Heat of mixing ΔH [see Eq. (2)] for random $\mathrm{Au}_x\mathrm{Pd}_{1-x}$. Note that ΔH does not contain Madelung terms with respect to ordered structures.

reduced to zero temperature. The figure shows that both the experimental data and the theoretical results produce a variation of the lattice constant with concentration with a break at about 30% and about 60% Au. The theoretical values for Au-rich alloys ($c_{\mathrm{Au}} > 0.60$) differ by less than 0.5% from the experimental data; for Pd-rich alloys this deviation is slightly bigger. As already mentioned, the breaks in the lattice constants are expected, by inference, from the position of the Fermi energy. For $0.3 \leq c_{\mathrm{Au}} \leq 0.6$ the variation of the theoretical lattice constants with respect to concentration is less than in the experiment and is probably due to the very sharp peak in the Pd PDOS in the vicinity of the Fermi energy (see also Fig. 1 of Ref. 12). On the other hand, experimental data (x-ray diffraction) give only an averaged position; additional experimental evidence might be required to explain the behavior of the lattice spacing in this range of concentrations.

Also marked in Fig. 2 are the positions of the minima of the component potential curves (a_0^{α},α = Au, Pd). On the Pd-rich side a_0^{Pd} increases with increasing Au concentration until about 50%, where both a_0^{Pd} and a_0^{Au} have about equal values. Above 60% Au, a_0^{Pd} decreases (almost linearly) with the concentration. As a consequence of the size of $\langle E_{\mathrm{Au}} \rangle$ and the weight of the Au component to the averaged total energy $\langle E \rangle$, for $c_{\mathrm{Au}} > 0.60$, the values of a_0^{Au} are only marginally larger than a_0. In the concentration regime between the two breaks for the lattice constants, namely $0.30 \leq c_{\mathrm{Au}} \leq 0.60$, a_0^{Au} nearly stays constant. Only below 30% Au does the Pd contribution to $\langle E \rangle$ carry enough weight to lower the theoretical prediction of a_0. It seems, using a kind of metallurgical language for a moment, that the Au component can only be squeezed to a certain extent, while the Pd component can only be pulled apart to some extent. This crossover is governed by the concentration and therefore the alloy lattice spacing at which the Fermi energy hits the d band from above. The different behavior of the components Au and Pd also has consequences for the concentration-dependent potential curves of $\langle E \rangle$. For $c_{\mathrm{Au}} > 0.60$ the compressive part (smaller lattice constant) shows a regime of lattice spacings, in which the potential curve is flatter than one would expect from the harmonic approximation; for $c_{\mathrm{Au}} < 0.40$ it is the expansive part that is affected by this kind of anharmonicity. Quite obviously the latter one is numerically much more difficult to handle. The potential curves for the components give an interesting view of the alloying process. It should be noted, however, that in principle only the averaged total energy is well defined.

In Fig. 3 the heat of mixing ΔH for the random alloy is shown,

$$\Delta H = \sum_{\alpha=A,B} c_\alpha \left[\min\langle E_\alpha(c_\alpha, a) \rangle - \min E_\alpha^0(a) \right], \quad (2)$$

where the $E_\alpha^0(a)$ are the total energies of the pure metals and the minimum is taken with respect to the lattice spacing a. The heat of mixing for the random alloy has a minimum at 60% Au of about 12 mRy, and a kind of shoulder at about 35%, namely, at that concentration where the Fermi energy moves through the above mentioned sharp peak in the Pd DOS. Since the calculation of ΔH involves differences of very large numbers, it is indeed a very delicate quantity. In particular the evaluation of $\min E_\alpha^0(a)$ on the same numerical footing as in the alloy calculation is of crucial importance. In the present calculation the functions $\min\langle E_\alpha(c_\alpha, a) \rangle, \alpha$ = Au,Pd, were extrapolated to the respective pure metals.

It should be noted that in none of the total energies in (2) is a Madelung term involved, since by definition within the single-site approximation to the CPA (see, for example, Ref. 1 or Ref. 7) there is no such term. Quite clearly, the true heat of mixing is modulated by Madelung terms due to existing ground state structures. These Madelung terms can be estimated from the component muffin-tin charges in terms of the usual approaches to electrostatics, provided the exact ordering is known or can be predicted either in terms of ordering energies[13] or in terms of Monte Carlo calculations based on the Ising model.[14] The heat of mixing for the ordered alloys has to reflect these Madelung contributions.

C. Linear coefficient of the specific heat

In Fig. 4 the bare DOS at the Fermi energy is shown in comparison to available experimental data for the linear

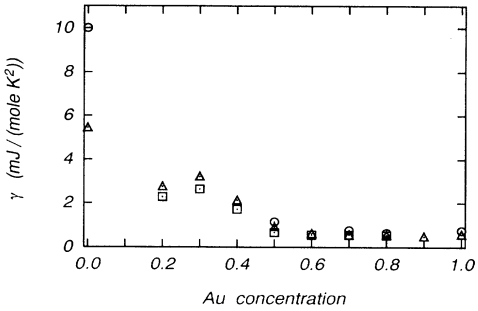

FIG. 4. Linear coefficient of the specific heat as obtained from the $l_{max} = 2$ (triangles) and $l_{max} = 3$ (squares) bare DOS at E_f in comparison to available experimental data (asterisks) (Refs. 4 and 24). For comparison for the pure metals the values of Moruzzi, Janak, and Williams (Ref. 15) (Pd) and Weinberger (Ref. 16) (Au) are shown.

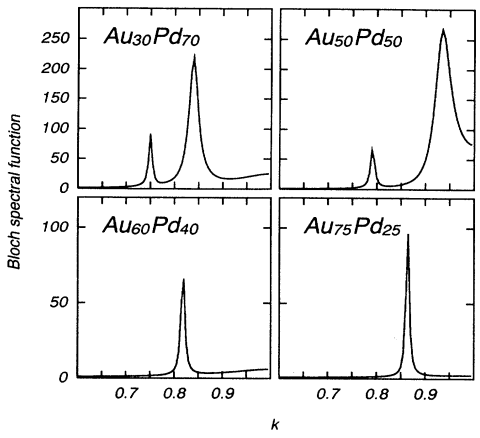

FIG. 5. $l_{max} = 3$ Bloch spectral functions at E_f along the direction [100] for $Au_{30}Pd_{70}$ ($a = 7.45$ a.u.), $Au_{50}Pd_{50}$ ($a = 7.50$ a.u.), $Au_{60}Pd_{40}$ ($a = 7.55$ a.u.), and $Au_{75}Pd_{25}$ ($a = 7.60$ a.u.). k is in units of π/a.

coefficient of the specific heat γ.[4,24] In both theoretical cases, namely the $l_{max} = 2$ and the $l_{max} = 3$ calculations, the values shown correspond to the calculated equilibrium lattice constants displayed in Fig. 2. As one can see from Fig. 4, both theoretical calculations describe the break in γ around 60% quite well, although the $l_{max} = 3$ calculation predicts this to occur at a lower concentration (around 55% Au). For comparison for pure Pd the value of Moruzzi, Janak, and Williams[15] is shown; for pure Au, that of Ref. 16. Note that the concentration at which the Fermi energy passes through the very sharp top peak in the Pd DOS can also be read off from Fig. 4.

When comparing experimental data with calculations for the electronic contribution to the specific heat, which use a bare DOS, one should remember that the theoretical treatment does not include (1) electron-phonon interactions (for a theoretical fully relativistic evaluation in terms of the rigid muffin-tin approximation (see Refs. 17 or 7), (2) spin fluctuations in the Pd-rich side of the alloy composition. Finally, when comparing results from a zero temperature theory to data measured at finite temperatures (and extrapolated to zero temperature) one should remember that the usual free electron theory formulation neglects a correction term involving the variation of the density of states with respect to energy. This is given by the following expression:

$$\gamma = \frac{[\pi k]^2}{3} n(E_f) \left\{ 1 - \left[\frac{kTn'(E_f)}{n(E_f)} \right]^2 \right\}, \qquad (3)$$

where $n(E_f)$ and $n'(E_f)$ are the density of states and its energy derivative evaluated at the Fermi energy (see e.g., Ref. 18). The importance of this correction involves the term with $n'(E_f)$ and the fact that, for materials where the density of states is a rapidly changing function of energy, it may not be negligible when extrapolating data to zero temperature.

D. Fermi vectors

It is very informative to follow the Bloch spectral functions[19,7] at the Fermi energy as they change with the concentration. In Fig. 5 these functions along the [100] direction are displayed for $Au_{30}Pd_{70}$ ($a = 7.45$ a.u.), $Au_{50}Pd_{50}$ ($a = 7.50$ a.u.), $Au_{60}Pd_{40}$ ($a = 7.55$ a.u.), and $Au_{75}Pd_{25}$ ($a = 7.60$ a.u.). One can see from this figure that for $c_{Au} \geq 0.60$ there is one rather sharp peak, the width of which is small compared to the length of the Brillouin zone vector in this direction. This indicates that for $c_{Au} \geq 0.60$ the system Au/Pd has a well-defined Fermi surface. The peak itself refers to an sp-like state of Δ_6 symmetry (relativistic point group symmetry). For $c_{Au} < 0.60$, in the neighborhood of [100], the Fermi surface is quite well defined. However, in this regime of concentrations, two rather sharp peaks are present, which rapidly move to smaller values of k as c_{Au} decreases. The peak at smaller values of k corresponds to the sp-like state of Δ_6 symmetry, whereas the second much broader peak corresponds to d-like states of Δ_6 and Δ_7 symmetry. The positions of sufficiently sharp peaks in the Bloch spectral functions are usually termed Fermi vectors in alloy theory.

In Fig. 6 a comparison of the ($l_{max} = 3$) Fermi vector along [110] is shown as related to diffuse electron scatter-

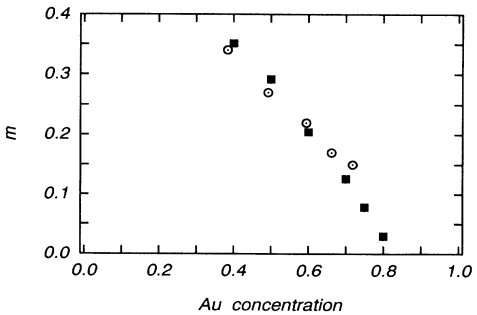

FIG. 6. Separation m of the split diffuse scattering maxima as measured in terms of the distance between the (000) and (200) fundamental scattering spots: experimental values (triangles) (Ref. 20), theoretical $l_{max} = 3$ values (squares).

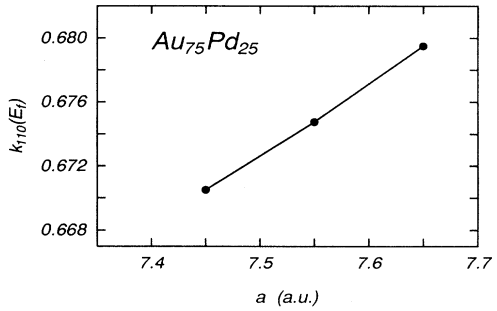

FIG. 7. Change of the Fermi vector (in units of π/a) along [110] in $Au_{75}Pd_{25}$ with respect to the lattice constant.

ing data by means of the "Krivoglaz" construction:[21,22]

$$m = |\mathbf{k}_{110}| - 2\,|\mathbf{k}_{110}(E_f)| = \sqrt{2} - 2\,|\mathbf{k}_{110}(E_f)|\ , \qquad (4)$$

where m is the separation of the split diffuse scattering maxima as measured in terms of the distance between the (000) and (200) fundamental scattering spots.[20] The calculated values of m (4) seem to be in reasonably good agreement with experiment.

Quite important for the so-called "$2k(E_f)$" theory (4) is the pressure or lattice parameter dependence of the Fermi vectors along the [110] direction. The critical temperatures of order-disorder phase transformations are usually at several hundred kelvins, which implies that the temperature dependence of the lattice parameters should be taken into account. As an example, Fig. 7 shows the lattice parameter dependence of this Fermi vector for the case of $Au_{75}Pd_{25}$. As one can see from this figure, the variation of the Fermi vector over about 0.5 a.u. is only about 1%. In this particular case, this variation is definitely of minor importance for the ordering problem.

IV. CONCLUSION

In the present paper a detailed study of total energies for the system Au/Pd was presented. Quite clearly not all available theoretical results could be discussed in full detail. To our knowledge, these calculations are the first self-consistent, fully relativistic, all-electron treatment for disordered alloys.

A few critical comments need to be stated at the end of this study. The $l_{\max} = 2$ calculation reproduced spectral densities surprisingly well, since these densities primarily map the underlying dispersion. For the purpose of comparing with angularly integrated spectroscopy (taking into account the limit of experimental resolution) $l_{\max} = 2$ calculations provide sufficient accuracy for good agreement with experiment.[12] In terms of the Ising model, up to now only $l_{\max} = 2$ calculations of effective pair and multisite interactions, needed for Monte Carlo studies that generate *ab initio* phase diagrams, have been performed.[13,14] In most cases the errors introduced by considering only coherent phase diagrams are probably larger than all possible modifications due to $l_{\max} = 3$ effects. However, for total energies and equilibrium lattice constants a high enough l expansion is essential, with $l_{\max} = 3$ being a minimum requirement for d-electron systems. Going beyond this value is probably unnecessary, at least for cubic systems, since errors due to the muffin-tin geometry should also be taken into account.

ACKNOWLEDGMENTS

The work presented in this paper was supported by grants from the Austrian Science Foundation (P7996) and the Austrian Ministry of Science (GZ 49.731/2-24/91). Most of the calculations were performed using the facilities of the University of Vienna computing center. It is a pleasure to thank Dr. P. Marksteiner for his computational advice and J. Fritscher for his PVM assistance.

[1] D.D. Johnson, D.M. Nicholson, F.J. Pinski, B.L. Gyorffy, and G.M. Stocks, Phys. Rev. B **41**, 9701 (1990); B.L. Gyorffy, D.D. Johnson, F.J. Pinski, D.M. Nicholson, and G.M. Stocks, in *Alloy Phase Stability*, Vol. 163 of *NATO Advanced Study Institute Series E: Applied Sciences*, edited by G.M. Stocks and A. Gonis (Kluwer Academic, London, 1989).

[2] H. Müller, H. Kirchmayr, P. Weinberger, and J. Redinger, Z. Phys. B **67**, 193 (1987).

[3] E. Arola, C.J. Barnes, R.S. Rao, and A. Bansil, Phys. Rev. B **42**, 8820 (1990).

[4] C. Schmitzer and G. Hilscher (private communication).

[5] M. Hansen, *Constitution of Binary Alloys* (McGraw-Hill, New York, 1958); E.M. Savitskii, V.P. Polyakova, and M.A. Tylkina, *Palladium Alloys* (Primary Sources, New York, 1969).

[6] J.B. Staunton, B.L. Gyorffy, and P. Weinberger, J. Phys. F **10**, 2665 (1980).

[7] P. Weinberger, *Electron Scattering Theory for Ordered and Disordered Matter* (Clarendon, Oxford, 1990).

[8] W.H. Fehlner and S.H. Vosko, Can. J. Phys. **54**, 2159 (1976).

[9] B. Ginatempo and J.B. Staunton, J. Phys. F **18**, 1827 (1988).

[10] P. Lloyd and P.V. Smith, Adv. Phys. **21**, 69 (1972).

[11] D.D. Johnson, D.M. Nicholson, F.J. Pinski, B.L. Gyorffy, and G.M. Stocks, Phys. Rev. Lett. **56**, 2088 (1986).

[12] P. Weinberger, L. Szunyogh, and B.I. Bennett, Phys. Rev. B **47**, 10 154 (1993).

[13] P. Weinberger, C. Blaas, B.I. Bennett, and A.M. Boring, Phys. Rev. B **47**, 10 158 (1993).

[14] P. Weinberger, L. Udvardi, and L. Szunyogh (unpublished).

[15] V.L. Moruzzi, J.F. Janak, and A.R. Williams, *Calculated Electronic Properties of Metals* (Pergamon, New York, 1978).

[16] P. Weinberger, J. Phys. F **12**, 2171 (1982).

[17] W. John, V.N. Nemoshkalenko, V.N. Antonov, and VI.N. Antonov, Phys. Status Solidi B **99**, 599 (1980).

[18]C. Kittel, *Introduction to Solid State Physics* (Wiley, New York, 1956), pp. 256-258.
[19]J.S. Faulkner and G.M. Stocks, Phys. Rev. B **23**, 5623 (1981); J.S. Faulkner, Prog. Mater. Sci. **27**, 1 (1982).
[20]K. Ohshima and D. Watanabe, Acta Crystallogr. A **33**, 784 (1977).
[21]M.A. Krivoglaz, *Theory of X-ray and Thermal Neutron Scattering by Real Crystals* (Plenum, New York, 1969).
[22]B.L. Gyorffy and G.M. Stocks, Phys. Rev. Lett. **50**, 374 (1983).
[23]O. Gunnarsson and B.I. Lundqvist, Phys. Rev. B **13**, 4274 (1976).
[24]K. Gschneider, Solid State Phys. **16**, 275 (1964).